Toxicology 441 (2020) 152493

Contents lists available at ScienceDirect

Toxicology

journal homepage: www.elsevier.com/locate/toxicol

Mechanism-based identification of plasma metabolites associated with liver toxicity

Venkat R. Pannala[a,b,*], Shanea K. Estes[c], Mohsin Rahim[d], Irina Trenary[d], Tracy P. O'Brien[c], Chiyo Shiota[c], Richard L. Printz[c], Jaques Reifman[a], Tatsuya Oyama[a,b], Masakazu Shiota[c], Jamey D. Young[c,d,**], Anders Wallqvist[a,*]

[a] Department of Defense Biotechnology High Performance Computing Software Applications Institute, Telemedicine and Advanced Technology Research Center, U.S. Army Medical Research and Development Command, Fort Detrick, MD 21702, USA
[b] The Henry M. Jackson Foundation for the Advancement of Military Medicine, Inc., Bethesda, MD 20817, USA
[c] Department of Molecular Physiology and Biophysics, Vanderbilt University School of Medicine, Nashville, TN 37232, USA
[d] Department of Chemical and Biomolecular Engineering, Vanderbilt University School of Engineering, Nashville, TN 37232, USA

ARTICLE INFO

Keywords:
Hepatotoxicants
Biomarker
Genome-scale models
Acetaminophen
Bromobenzene
Pathways

ABSTRACT

Early diagnosis of liver injuries caused by drugs or occupational exposures is necessary to enable effective treatments and prevent liver failure. Whereas histopathology remains the gold standard for assessing hepatotoxicity in animals, plasma aminotransferase levels are the primary measures for monitoring liver dysfunction in humans. In this study, using Sprague Dawley rats, we investigated whether integrated analyses of transcriptomic and metabolomic data with genome-scale metabolic models (GSMs) could identify early indicators of injury and provide new insights into the mechanisms of hepatotoxicity. We obtained concurrent measurements of gene-expression changes in the liver and kidneys, and expression changes along with metabolic profiles in the plasma and urine, from rats 5 or 10 h after exposing them to one of two classical hepatotoxicants, acetaminophen (2 g/kg) or bromobenzene (0.4 g/kg). Global multivariate analyses revealed that gene-expression changes in the liver and metabolic profiles in the plasma and urine of toxicant-treated animals differed from those of controls, even at time points much earlier than changes detected by conventional markers of liver injury. Furthermore, clustering analysis revealed that both the gene-expression changes in the liver and the metabolic profiles in the plasma induced by the two hepatotoxicants were highly correlated, indicating commonalities in the liver toxicity response. Systematic GSM-based analyses yielded metabolites associated with the mechanisms of toxicity and identified several lipid and amino acid metabolism pathways that were activated by both toxicants and those uniquely activated by each. Our findings suggest that several metabolite alterations, which are strongly associated with the mechanisms of toxicity and occur within injury-specific pathways (e.g., of bile acid and fatty acid metabolism), could be targeted and clinically assessed for their potential as early indicators of liver damage.

1. Introduction

The liver is one of the five vital organs necessary for human survival. Its essential functions include protein synthesis, glucose storage and synthesis, hormone production, and bile synthesis. Importantly, because the liver plays a major role in the metabolism and detoxification of drugs and environmental chemicals, it is one of the organs most susceptible to chemical injuries when endogenous defense mechanisms become overwhelmed and/or contribute to the generation of toxic metabolites. Several biomarkers are currently used to clinically diagnose and monitor liver dysfunction, disease, and incipient failure. The most commonly used non-invasive biomarkers include two aminotransferases, alanine aminotransferase (ALT) and aspartate aminotransferase (AST) (Kim et al., 2008; Pratt and Kaplan, 2000). Other biomarkers include alkaline phosphatase, total bilirubin, gamma-glutamyl transferase, total serum protein, and prothrombin time (Kaptanoglu et al., 2017; Ozer et al., 2008; Ramachandran and Kakar, 2009; Shi et al., 2010). Yet, these markers, which are useful in clinical

* Corresponding authors at: Department of Defense Biotechnology High Performance Computing Software Applications Institute, Telemedicine and Advanced Technology Research Center, U.S. Army Medical Research and Development Command, Fort Detrick, MD 21702, USA.
** Corresponding author at: Department of Chemical and Biomolecular Engineering, Vanderbilt University School of Engineering, Nashville, TN 37232, USA.
E-mail addresses: vpannala@bhsai.org (V.R. Pannala), j.d.young@vanderbilt.edu (J.D. Young), sven.a.wallqvist.civ@mail.mil (A. Wallqvist).

https://doi.org/10.1016/j.tox.2020.152493
Received 6 March 2020; Received in revised form 1 May 2020; Accepted 8 May 2020
Available online 30 May 2020
0300-483X/

practice, still have notable shortcomings (Senior, 2012). For example, ALT and AST do not necessarily correlate with outcome in patients with drug-induced liver injury (McGill et al., 2014), and although typically elevated only in the late stages of disease, may not be elevated in some cases despite histological evidence of disease progression (Marcellin et al., 1997; Nallagangula et al., 2018; Roshan and Guzman, 2014).

Given these limitations, there is a need to identify additional biomarkers that can be measured in conjunction with, or altogether outperform, current biomarkers (Drescher et al., 2019; Eguchi et al., 2014; McGill and Jaeschke, 2019; Vilar-Gomez and Chalasani, 2018). One promising approach to identify such biomarkers is to search for indicators of pathophysiological mechanisms (McGill and Jaeschke, 2014). These indicators can appear in circulation early in the course of tissue injury, because any event that contributes to the damage must occur before the injury appears. However, for most toxicants, the metabolites they generate and their toxicity mechanisms are unknown. Although most drugs and environmental chemicals are not intrinsically toxic to the liver, they can cause injury when they are bioactivated through the production of secondary metabolites. The liver plays a critical role in xenobiotic metabolism and promotes the excretion of these compounds by transforming them into metabolites with increased water solubility (Sturgill and Lambert, 1997). These functions are carried out in the centrilobular hepatocytes by cytochrome P450 enzymes, a supergene family of heme-containing, and mixed-function oxidase enzymes (Watkins, 1992). The reactions these enzymes facilitate have the potential to induce cellular injury via several toxicity mechanisms. For example, P450-mediated oxidation of bromobenzene (BB) and acetaminophen (APAP) generates highly electrophilic intermediate compounds capable of forming covalent adducts with critical cellular macromolecules that regulate calcium homeostasis, such as thiol-containing membrane proteins (Bellomo and Orrenius, 1985). The resulting induction of increased intracellular calcium may be one common pathway by which such reactions lead to cell death. Furthermore, the conjugation of secondary toxic metabolites depletes the hepatic glutathione (GSH) pool, thereby reducing intracellular protection against reactive oxygen species (ROS). This may lead to several deleterious events that damage the cell, including lipid peroxidation, ATP depletion, and mitochondrial dysfunction (Benedetti et al., 1986; Locke and Brauer, 1991). Therefore, monitoring changes in injury-specific pathways might provide mechanistic indicators that are common to several liver-specific disease processes.

Several promising candidate mechanistic markers have been identified based on models of APAP-induced liver injury. For example, glutamate dehydrogenase (GLDH), a mitochondrial enzyme found primarily in the liver, is more tissue-specific than ALT or AST (Antoine et al., 2013). Similarly, high-mobility group box 1 (HMGB1), a chromatin-binding protein with proinflammatory activity, and keratin-18 (K18), a member of the keratin protein family, have been identified as blood-based markers that are more sensitive than ALT (Antoine et al., 2012). Several other studies have reported changes in serum microRNA (miRNA) concentrations at an early stage of liver injury, which are more specific to the liver than are changes in ALT (Starkey Lewis et al., 2011; Thulin et al., 2014). In particular, miR-122 and miR-192 were the first circulating miRNAs shown to increase after administration of toxic doses of APAP, initially in mice and soon after in human subjects (Wang et al., 2009). Although these emerging biomarkers show promise of early injury detection and organ specificity, they have yet to be introduced into clinical practice. Furthermore, the heterogeneity of responses to toxic chemicals or drugs among individuals, and the multitude of pathways contributing to hepatic injury, make it unlikely that any single protein or biomolecule will be sufficient as an early injury indicator (Campion et al., 2013). Therefore, multiplexed panels of biomolecules will likely have greater applicability across a wide range of drug- or chemical-induced liver-injury scenarios (Alfirevic and Pirmohamed, 2012).

High-throughput technologies, such as transcriptomics and metabolomics, hold promise for identifying interrelated changes in multiple genes and metabolites induced by hepatotoxic chemicals (Beger et al., 2010; Heinloth et al., 2007). The ability to monitor a large number of interdependent molecules (genes and metabolites) in tissues and accessible biofluids can potentially provide information on the underlying mechanisms of distinct forms of liver injury. Creating and implementing such data- and modeling-driven approaches would enable the discovery of early diagnostic markers based on mechanistic considerations. Because gene-expression changes influence biochemical reactions, which in turn determine metabolite levels, a systems-level approach that combines transcriptomics and metabolomics could allow us to systematically analyze these changes associated with liver injuries. However, it remains to be seen whether we can link changes in mRNA at the transcriptomic level to tissue-specific metabolite alterations detectable in biofluids, such as blood and urine. To this end, genome-scale metabolic models (GSMs) have proven to be a suitable platform for integrating high-throughput data to elucidate genotype-phenotype relationships and identify biological processes associated with disease states (Baloni et al., 2019; Blais et al., 2017; Gille et al., 2010; Jerby et al., 2010; Mardinoglu et al., 2014; Pannala et al., 2020; Rawls et al., 2019; Vinnakota et al., 2019). In our previous work, we have used GSMs to identify plasma and urine metabolite signatures that are strongly correlated with gene-expression changes in the liver and kidneys induced by APAP and gentamicin, respectively (Pannala et al., 2020, 2019; Pannala et al., 2018). These studies also demonstrate that GSM analysis of gene expression and metabolite profiles can provide mechanistic insights into APAP-induced liver toxicity and gentamicin-induced kidney toxicity.

In this study, we investigated the relationship between the gene-expression profiles and metabolic phenotypes of two hepatotoxic chemicals, as measured by RNA-sequencing, metabolic profiling, and $^{2}H/^{13}C$ metabolic flux analysis. We selected the routinely used hepatotoxicants APAP and BB, which deplete cellular GSH pools by conjugation reactions and cause cell death (Heijne et al., 2003). Using male Sprague Dawley rats, we acquired liver and kidney transcriptomes, plasma and urine metabolomes, and absolute hepatic flux changes in central carbon metabolism, to capture changes occurring at the systems level. We then analyzed the experimental data and integrated them with a multi-tissue GSM to identify the correlation between biochemical markers and gene-expression profiles for the two chemicals. Our analyses revealed that the expression profiles of liver genes and plasma metabolites induced by administration of APAP and those induced by administration of BB were highly correlated ($r = 0.90$ and 0.60 for the expression profiles of liver genes and plasma metabolites, respectively) regardless of the time of assessment (5 or 10 h). Furthermore, our GSM-based analysis provided several mechanistic insights into the liver toxicity induced by APAP and BB, with similar genomic perturbations in several lipid and carbohydrate metabolism pathways, as well as distinct perturbations in amino acid-related and nucleotide metabolism pathways. We also identified a potential panel of metabolites that could be measured in the plasma to detect liver injury in the early stages of disease progression. Of the total number of metabolites that significantly changed in the plasma and mapped to the GSM, for approximately 60 %, the changes strongly correlated with changes in gene expression in the liver. Our work suggests that these metabolite alterations are strongly tied to the mechanisms of injury and, therefore, could be targeted and clinically assessed for their potential to serve as early indicators of liver damage.

2. Materials and methods

2.1. Animals and study design

We carried out the experiments in accordance with the *Guide for the Care and Use of Laboratory Animals* of the United States (U.S.) Department of Agriculture and the National Institutes of Health, after

obtaining protocol approval from the Vanderbilt University Institutional Animal Care and Use Committee and the U.S. Army Medical Research and Development Command Animal Care and Use Review Office. We purchased male Sprague Dawley rats at 10 weeks of age (approximately 280–320 g) from Charles River Laboratories (Wilmington, MA) and housed them under environmentally controlled conditions (12:12-h light-dark cycle at 23 °C). We gave the rats free access to water and a commercially available rodent diet, Formulab Diet 5001 (LabDiet, Richmond, IN), and allowed them to acclimatize to the housing conditions for a week. Seven days before each experiment, we anesthetized the rats with isoflurane and performed a catheter implantation surgery for sample collection. We refer the reader to details of this procedure in our recent publications (Pannala et al., 2020, 2019; Pannala et al., 2018).

2.2. Preliminary studies for determining appropriate dose and time of assessment

Two days before each study, we moved the rats from their regular housing cages to metabolic cages (Harvard Apparatus, Holliston, MA). To determine the appropriate dose of BB and the time of assessment after exposure, following an initial collection of blood, we administered to rats either vehicle (5 mL/kg of corn oil, n = 4) or BB (0.2, 0.4 or 0.6 g/kg, n = 4 per dose) by gavage at 7 a.m. Subsequently, we collected blood and accumulated urine samples at 11 a.m., 3 p.m., and 7 p.m. on the first day, and then at 7 a.m., 11 a.m., 3 p.m., and 7 p.m. on the second day. During the study period, animals were allowed access to water and food *ad libitum* (Fig. 1A). To evaluate liver injuries, we measured the plasma levels of ALT and AST using the corresponding activity assay kits (Sigma-Aldrich, St Louis, MO). Similarly, to evaluate kidney injuries, we measured kidney-injury molecule-1 (KIM-1) using the KIM-1 Rat ELISA kit (Abcam Inc., Cambridge, MA). We used a two-way analysis of variance method to compare mean differences between the dose and time points and to understand if there is an interaction between dose and time for the ALT and AST measurements.

We included some results from a previous APAP study (Pannala et al., 2019), in which following an initial collection of blood, we administered to rats either vehicle (6 mL/kg of 50 % polyethylene glycol, n = 6) or APAP (1 or 2 g/kg, n = 6 per dose) by gavage at 7 a.m. We then collected samples of blood and accumulated urine at 5 p.m. on the first day, and then at 7 a.m. and 5 p.m. on both the second and third days. During the study period, animals were allowed access to water and food *ad libitum* (Fig. 1B).

2.3. Studies for measuring changes in gene-expression and biofluid metabolite profiles

Based on the results of the dose-response study, we selected 0.4 g/kg and 2 g/kg as the appropriate doses for BB and APAP, respectively, and two assessment times after exposure, one short (5 h, n = 8) and the other long (10 h, n = 8), to obtain transcriptomic and metabolomic data (Fig. 1C). For each study, following an initial collection of blood, we gave animals either vehicle or one of the toxicants (BB or APAP) at 7 a.m., and then moved them to new housing cages where they could access water *ad libitum* but not food. We collected blood samples from the 5-h study at 12 p.m. and from the 10-h study at 5 p.m., centrifuged the collected samples immediately, and froze the separated plasma samples on dry ice. We collected urine samples directly from the bladder and froze them immediately on dry ice. Subsequently, we anesthetized these animals with an intravenous injection of sodium pentobarbital through the jugular vein catheter, and then immediately subjected them to a laparotomy. We removed the liver and kidneys and froze them using Wollenberger tongs precooled in liquid nitrogen. The sample collection process required only seconds. Prior to analyses, we stored the plasma, urine, and organ samples in a −80 °C freezer.

2.4. Studies for measuring metabolite flux

At 7 a.m. on the day of the study, we administered either BB (0.4 mg/kg, n = 8) or vehicle (corn oil, 5 mL/kg, n = 8); for the APAP study, we administered either APAP (2 g/kg, n = 8) or vehicle (6 mL/kg of 50 % polyethylene glycol, n = 8) (Fig. 1D). We then transferred the animals to new housing cages, where they were allowed access to water *ad libitum* but not food. At 12:50 p.m., we anesthetized the animals with isoflurane and, during this short period of anesthesia (approximately 5 min), collected 200 µL of arterial blood through the carotid artery catheter to determine the natural isotopic abundance of circulating glucose, after which we subcutaneously administered a bolus of [$^2H_2$] water (99.9 %) containing 0.9 % sodium chloride to enrich total body water to 4.5 %. After they had recovered from anesthesia, we placed the rats in bedded containers without food and water, and then connected them to sampling and infusion lines. At 1 p.m. (i.e., 6 h after toxicant administration), we delivered [6,6-$^2H_2$] glucose (80 mg/kg prime +0.8 mg/kg/min infusion) as a prime-constant infusion into the systemic circulation through the jugular vein catheter for the duration of the study. Starting 120 min after the [$^2H_2$] water bolus, we delivered sodium [$^{13}C_3$] propionate (99 %) as a prime-constant infusion (110 mg/kg +5.5 mg/kg/min infusion). We prepared all infusates in a 4.5 % [$^2H_2$] water-saline solution unless otherwise specified, and obtained stable isotopes from Cambridge Isotope Laboratories (Tewksbury, MA). At each of three time points during the last 20 min of the tracer-infusion period (100, 110, and 120 min from the start of the infusion), we collected a 300-µl arterial blood sample in an EDTA-coated tube. We centrifuged the collected blood samples immediately to isolate plasma samples, which we stored at −80 °C prior to any glucose derivatization and gas chromatography-mass spectrometry (GC–MS) analysis. Immediately after collecting the final steady-state sample, we quickly euthanized the rats by injecting sodium pentobarbital through the carotid artery catheter. We collected post-study samples as described in the previous section.

2.5. Preparation of glucose derivatives and GC–MS analysis

We divided the plasma samples into three aliquots and derivatized each separately to obtain di-*O*-isopropylidene propionate, aldonitrile pentapropionate, and methyloxime pentapropionate derivatives of glucose. To prepare di-*O*-isopropylidene propionate, we precipitated proteins from 20 µL of plasma using 300 µL of cold acetone, and then evaporated the protein-free supernatant to dryness in screw-cap culture tubes. Derivatization proceeded as previously described (Antoniewicz et al., 2011) to produce glucose 1,2,5,6-di-isopropylidene propionate. For aldonitrile and methyloxime derivatization, we precipitated proteins from 10 µL of plasma using 300 µL of cold acetone and evaporated the protein-free supernatants to dryness in microcentrifuge tubes. Derivatizations then proceeded as described previously (Antoniewicz et al., 2011) to produce glucose aldonitrile pentapropionate and glucose methyloxime pentapropionate. We evaporated all derivatives to dryness, dissolved them in 100 µL of ethyl acetate, and transferred them to gas chromatography (GC) injection vials with 250-µl glass inserts for GC–MS analysis. Subsequently, we performed GC–MS analysis using an Agilent 7890A GC system with an HP-5 MS capillary column (30 m ×0.25 mm ×0.25 µm; Agilent Technologies, Inc., Santa Clara, CA) interfaced with an Agilent 5975C Mass Spectrometer as previously described (Pannala et al., 2020, 2019).

2.6. $^2H/^{13}C$ metabolic flux analysis (MFA)

We employed the *in vivo* MFA methodology described previously (Hasenour et al., 2015; Pannala et al., 2018; Vinnakota et al., 2019). Briefly, we constructed a reaction network using the INCA software package (Young, 2014) and defined the carbon and hydrogen transitions for biochemical reactions linking hepatic glucose production and

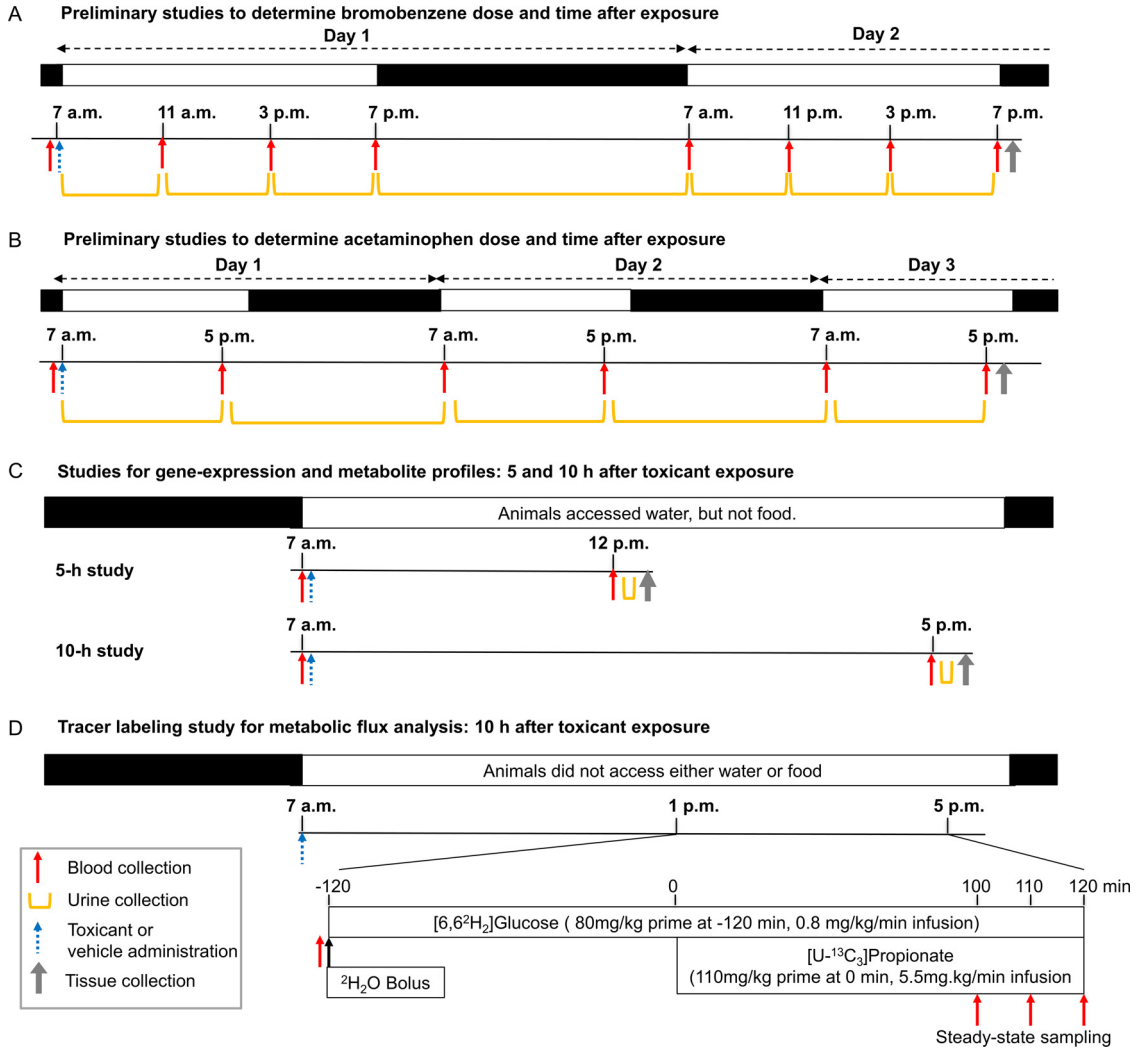

Fig. 1. Protocol to determine toxicant dose and time points to collect samples after exposure, and experimental design to measure early perturbations in rat metabolism. Schedule for (A) bromobenzene (BB) or (B) acetaminophen (APAP) administration by oral gavage and collection of blood, accumulated urine, and tissue samples for the preliminary studies. C) Experimental design to measure transcriptome and metabolome data. Before the experiment, we catheterized the rats and allowed them to recover for 1 week. At 7 a.m. on the day of sample collection, the rats received either BB (0.4 g/kg, n = 8) or APAP (2 g/kg, n = 8) while their corresponding controls received corn oil (for the BB study) or 50 % polyethylene glycol (for the APAP study; n = 8 each). Subsequently the collection of blood, urine, and tissue samples occurred at 12 p.m. for the 5-h study and 5 p.m. for the 10-h study. D) Design of isotope tracer labeling study to measure absolute fluxes in central carbon metabolism. Rats received either BB (0.4 g/kg, n = 8) or APAP (2 g/kg, n = 8) at 7 a.m., while their corresponding controls received either corn oil or 50 % polyethylene glycol (n = 8 each). Isotope tracer infusions began at 1 p.m. Blood sample collection occurred at 5 p.m. to obtain the isotope-labeling measurements required for metabolic flux analysis.

its associated intermediary metabolic reactions. INCA relies on the elementary metabolite unit method to simulate mass isotopomer distributions of measured metabolites and to regress the metabolic network model to fit the experimental measurements. We estimated the flux through each reaction relative to citrate synthase (fixed at 100) by minimizing the sum of squared residuals (SSRs) between the simulated and experimentally determined mass isotopomer distributions of the six fragment ions previously described, and repeated this process 50 times by randomizing the initial values. We iteratively adjusted the flux parameters of the model using a Levenberg–Marquardt algorithm until we obtained optimal agreement with experimental data. We used the chi-square test to assess goodness-of-fit, and computed 95 % confidence intervals (CIs) by evaluating the sensitivity of the SSRs to variations in flux values (Antoniewicz et al., 2006). The average SSR of each experimental group (APAP control: 22.69 ± 1.83; APAP: 27.73 ± 2.17; BB control: 33.64 ± 1.65; BB: 32.77 ± 1.55) fell within the 95 % CI [13.8, 41.9] of the corresponding chi-square distribution with 26 degrees of freedom (i.e., the regressions were overdetermined by 26 measurements). We converted the relative fluxes to absolute values using the known [6,6-$^{2}H_2$] glucose infusion rate and rat weights, and then averaged the flux estimates for the steady-state samples to obtain a representative set of values for each rat.

2.7. Metabolomic analysis

We carried out sample preparation at Metabolon, Inc. (Durham, North Carolina), in a manner similar to a previous study (Hatano et al., 2016). Briefly, this involved subjecting individual samples to methanol extraction and then splitting them into aliquots for analysis by ultra-high performance liquid chromatography/MS (UHPLC/MS). The global biochemical profiling analysis comprised four unique arms: a reverse-phase chromatography positive ionization method optimized for hydrophilic compounds (LC/MS Pos Polar), a corresponding method for hydrophobic compounds (LC/MS Pos Lipid), reverse-phase chromatography with negative ionization conditions (LC/MS Neg), and a hydrophilic interaction liquid chromatography (HILIC) method coupled to

negative ionization (LC/MS Polar) (Evans et al., 2014). All methods alternated between full scan MS and data-dependent MS^n scans. The scan range varied slightly between methods but generally covered mass-to-charge (m/z) values between 70 and 1000. The identification of metabolites involved automated comparison of the ion features in the experimental samples to those of a reference library of chemical standard entries, which included retention time, m/z, preferred adducts, in-source fragments, and associated MS spectra, followed by curation via visual inspection for quality control using software developed at Metabolon. Identification of known chemical entities was based on comparison with metabolomic library entries of purified standards (Dehaven et al., 2010).

We performed two types of statistical analyses: *1*) significance tests and *2*) classification analyses. For all statistical analyses, which were based on log-transformed data, we used ArrayStudio and customized programs in R (http://cran.r-project.org). Following log transformation and imputation of missing values (if any) with the minimum observed value for each compound, we used Welch's 2-sample *t*-test to identify biochemicals that differed significantly ($p < 0.05$) between experimental groups. We estimated the false discovery rate (FDR: q value) to correct for multiple comparisons.

2.8. RNA isolation, sequencing, and analysis

Because the kidneys are histologically heterogeneous, we powdered frozen whole kidney samples in liquid nitrogen. We isolated total RNA from the liver and powdered kidneys using TRIzol Reagent (Thermo Fisher Scientific, Waltham, MA) and the direct-zol RNA MiniPrep kit (Zymo Research, Irvine, CA). Subsequently, we submitted the isolated RNA samples to the Vanderbilt University Medical Center VANTAGE Core (Nashville, TN) for RNA quality determination and sequencing. Following total RNA quality assessment using a 2100 Bioanalyzer (Agilent), we used at least 200 ng of DNase-treated total RNA of high integrity to generate poly-A-enriched mRNA libraries using KAPA Stranded mRNA sample kits with indexed adaptors (Roche, Indianapolis, IN). We then assessed the quality of the libraries using a 2100 Bioanalyzer (Agilent) and quantitated them using KAPA library Quantification kits (Roche), respectively. We subjected the pooled libraries to 150-bp paired-end sequencing for the BB study (NovaSeq6000; Illumina, San Diego, California) and 75-bp single-end sequencing for the APAP study (HiSeq3000; Illumina, San Diego, California) according to the manufacturer's protocol. We used Bcl2fastq2 Conversion Software (Illumina) to generate de-multiplexed Fastq files.

We used the RNA-sequencing data analysis tool Kallisto for read alignment and quantification (Bray et al., 2016). Kallisto pseudo-aligns the reads to a reference, producing a list of transcripts that are compatible with each read while avoiding alignment of individual bases. In this study, we pseudo-aligned the reads to the *Rattus norvegicus* transcriptome (Rnor_6.0) downloaded from the Ensembl website (Cunningham et al., 2019). Kallisto achieves a level of accuracy similar to that of other competing methods, but is orders of magnitude faster. Its speed allows for the use of a bootstrapping technique to calculate uncertainties of transcript abundance estimates by repeating the analyses after resampling with replacement. Here, we employed this technique to repeat the analysis 100 times. The raw and processed RNA-seq data, which we have deposited in NCBI's Gene Expression Omnibus (GEO) database, are available under series accession number GSE148853.

To identify differentially expressed genes (DEGs) from transcript abundance data, we used Kallisto's companion analysis tool Sleuth, which uses the results of the bootstrap analysis during transcript quantification to directly estimate the technical gene variance for each sample (Pimentel et al., 2017). Briefly, we first prepared an auxiliary table that describes the relationship between the Kallisto-derived abundance files to control and treatment samples and constructed a Sleuth object, which stores not only information about the experiment, but also details of the (full) model to be used for differential testing. We then performed a differential analysis using the Wald test to obtain the estimated logarithmic fold changes between treatment and control samples.

2.9. Rat multi-tissue model and algorithm for data integration and metabolite predictions

For our systems-level analyses, we used a recently developed rat multi-tissue model comprising the liver and kidney tissues connected with the blood and urine compartments (Pannala et al., 2020). We then used the transcriptionally inferred metabolic biomarker response (TIMBR) algorithm (Blais et al., 2017) to integrate the observed gene-expression changes in the liver and kidneys into the multi-tissue model and make predictions for metabolite alterations in the blood and urine. Briefly, the TIMBR algorithm uses the gene-protein-reaction (GPR) relationships in the model to convert the $\log_2$ fold changes of all liver- and kidney-specific alterations in gene expression into reaction weights. It then calculates the global network demand required for producing a metabolite in the blood and urine. The objective function minimizes the weighted sum of fluxes across all reactions for each condition and metabolite, to satisfy the associated mass balance and the optimal fraction of the maximum network capability to produce a metabolite. Based on values reported in the literature, we used appropriate uptake and secretion rates for the exchange reactions of the liver and kidney under short-term fasting conditions (Pannala et al., 2019). Thus, using the gene-expression changes together with the uptake and secretion rates, TIMBR provides a production score (z-score) that represents an increase or decrease for each metabolite in the plasma and urine.

We used the experimental $\log_2$ fold changes of significantly altered (FDR < 0.10) plasma and urine metabolites from the global metabolic profiling data and then compared the corresponding TIMBR production scores from the multi-tissue GSM at 5 or 10 h after each toxicant treatment. Here, we considered the metabolite levels as having increased or decreased based on TIMBR production score cut-off values of greater than 0.1 and smaller than –0.1, respectively. We considered metabolites with scores between –0.1 and 0.1 as unchanged. To test the robustness of the results from the multi-tissue model, we randomized the original gene-expression data by randomly sorting the gene names and using the resulting data as the input.

2.10. KEGG pathway analysis

To perform gene-enrichment analysis using KEGG pathways, we used the online tool Database for Annotation, Visualization, and Integrated Discovery (DAVID) (Huang et al., 2009) and a list of significantly altered metabolic genes for each toxicant as the input. In addition, we used the aggregated fold change (AFC) method (Yu et al., 2017), which calculates significantly enriched KEGG pathways together with their direction of change, to ascertain that the results were independent of the pathway-detection method. Briefly, the AFC method calculates the mean fold change for each gene and defines the KEGG pathway score as the average mean fold change of all genes in the pathway. The sign of the pathway score represents the direction of regulation, with positive values indicating up-regulation and negative values indicating down-regulation. Similarly, to understand the biological significance of metabolites, we identified those metabolites whose levels were significantly altered in the blood or urine and which mapped to the rat GSM as input, and used KEGG pathways to identify molecular pathways that were significantly enriched. We used the pathway analysis functionality in MetaboAnalyst 4 (Chong et al., 2018) to perform this task. Briefly, we selected the Pathway Analysis tab at MetaboAnalyst (https://www.metaboanalyst.ca/) to upload the compound names (or KEGG IDs) of metabolites detected in the plasma and urine. We then selected the hypergeometric test and relative

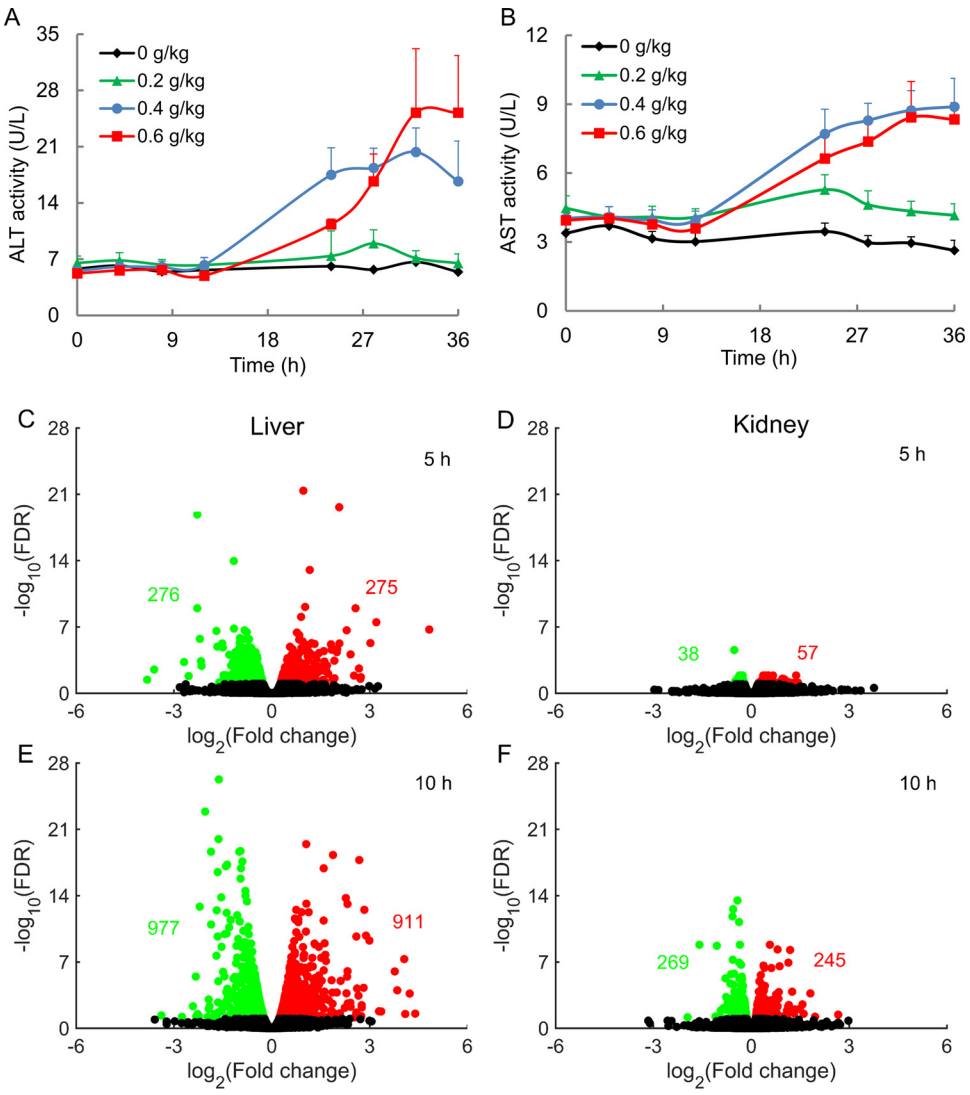

Fig. 2. Time course of levels of liver-injury markers in plasma and global changes in gene expression in the rat liver and kidneys. Changes in (A) plasma ALT and (B) AST levels in rats exposed to bromobenzene as a function of dose. Volcano plots for global gene-expression changes in the liver and kidney at 5 h (C and D) and 10 h (E and F) after bromobenzene exposure. Red and green dots indicate genes significantly up- and down-regulated [false discovery rate (FDR) < 0.1)], respectively, with their total numbers shown in the corresponding colors. Black dots represent unchanged genes. (For interpretation of the references to color in this figure legend, the reader is referred to the web version of this article.)

betweeness centrality to perform over-representation and pathway topology analyses, respectively. We used the KEGG pathways for *Rattus norvegicus* to identify significantly altered pathways and the metabolites within them for further analysis.

3. Results

3.1. Monitoring early toxicant-induced changes in liver and kidney metabolism

To capture early changes in liver and kidney metabolism, we first performed dose-response studies and identified the effective dose at which current markers show abnormalities in liver or kidney function. Fig. 2A and B show marked elevations in the levels of liver markers ALT and AST as a function of dose and time after BB exposure, clearly indicating the hepatotoxic nature of BB. However, BB exposure did not lead to elevations in urine levels of KIM-1 (data not shown). Twenty-four hours after BB administration, we observed peak ALT and AST levels that depended on the administered dose, with the highest dose resulting in the maximum perturbation relative to controls. For both enzyme levels, a two-way analysis of variance (ANOVA) with dose and time (from 0 up to 36 h after BB administration) as between-subject factors revealed a significant main effect of dose [$F(3, 96) = 12.5$, $p < 0.0001$ for ALT; $F(3, 96) = 40.4$, $p < 0.0001$ for AST], main effect of time [$F(7, 96) = 8.98$, $p < 0.0001$ for ALT; $F(7, 96) = 14.5$, $p < 0.0001$ for AST], and dose by time interaction [$F(21, 96) = 3.2$, $p < 0.0001$ for ALT; $F(21, 96) = 4.93$, $p < 0.0001$ for AST]. In contrast, for the first four time points (up to 12 h after BB administration), save for a dose effect on AST level due to a slight difference in the control compared to the other groups [$F(3, 48) = 10.1$, $p < 0.0001$], no other effect was significant. The trend was similar to that for liver markers in a previous APAP study, although the peak elevations occurred 48 h after APAP administration (Pannala et al., 2019). In both studies, neither of these markers showed significant elevation until 12 h after toxicant administration. Therefore, we selected 5 h and 10 h as the two early time points to measure changes in gene expression and metabolites after a single dose of either 0.4 g/kg of BB (for the BB study) or 2 g/kg of APAP (for the APAP study). Furthermore, given that maintaining glucose hemostasis is one of the major functions of the liver, under similar conditions we also examined the impact of toxicant exposure on central carbon metabolism.

3.2. Global gene-expression changes in the liver

Consistent with the well-known hepatotoxic effect of BB, our transcriptomic analysis revealed many significant gene-expression changes in the liver (Fig. 2C and E) but fewer changes in the kidney (Fig. 2D and F). Based on an FDR cut-off value of 0.10, we identified 551 (Fig. 2C) and 1888 (Fig. 2E) genes that significantly changed in the liver at 5 and 10 h, respectively, after BB administration. At each time point,

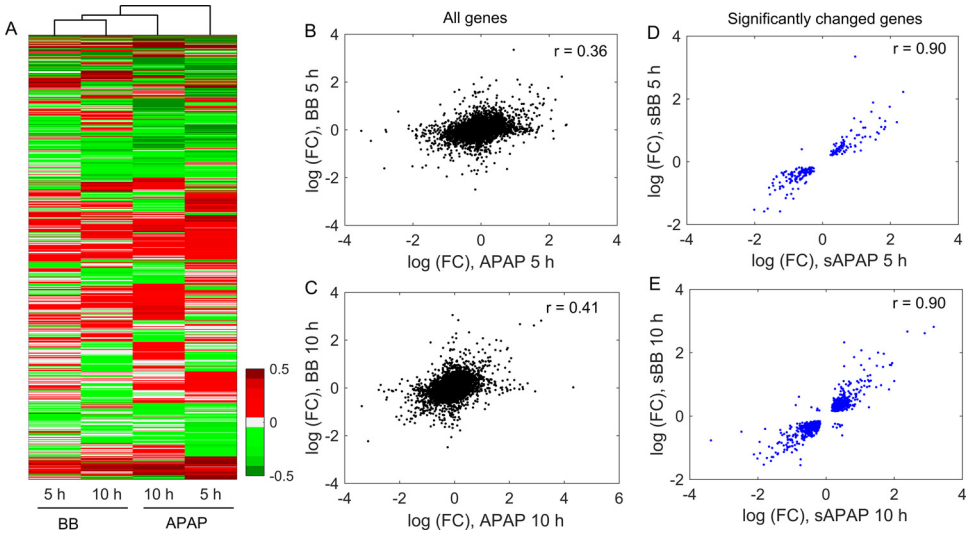

Fig. 3. Hierarchical clustering and correlation analyses of differentially expressed genes (DEGs) that were common between bromobenzene (BB) and acetaminophen (APAP). A) Clustering analysis of all common DEGs (fold changes relative to controls) in the rat liver 5 or 10 h after BB or APAP exposure. Red and green bars indicate up- and down-regulated DEGs, respectively; grey bars indicate unchanged genes. Correlations between the logarithmic fold changes of all DEGs induced by BB and those of all DEGs induced by APAP at 5 h (B) and 10 h (C) after toxicant exposure, and corresponding correlations for only significant DEGs (FDR < 0.1) at 5 h (D) and at 10 h (E). (For interpretation of the references to color in this figure legend, the reader is referred to the web version of this article.)

comparable numbers of DEGs were up- or down-regulated, with the 10-h time point after BB administration resulting in more DEGs with greater magnitudes of change, indicating a prolonged effect of BB on the liver. We provide a complete list of all DEGs in Supplementary Table S1. The results were similar for APAP, although the total number of DEGs in the liver was higher than for BB, with 1383 and 2551 genes at 5 and 10 h, respectively (Pannala et al., 2019). Interestingly, in both studies, several genes that changed significantly by the first time point (5 h) remained altered at the second time point (10 h), indicating persistent perturbations in liver metabolism (Supplementary Table S2).

To identify common changes in liver gene-expression profiles between the two toxicants, we performed hierarchical clustering analysis and identified the correlation between the observed changes at the two time points (Fig. 3). As expected, comparisons of gene-expression changes observed at both 5 and 10 h after toxicant exposure showed that the similarity between different time points for the same chemical was greater than the similarity between different chemicals at the same time point. Furthermore, when we compared the different chemicals, the gene-expression changes at 10 h were more closely clustered together than were those at 5 h (Fig. 3A). We observed a low correlation between APAP and BB (0.36 and 0.41 for the 5- and 10-h study groups, respectively) when we used all gene-expression changes irrespective of their significance level (Fig. 3B and C). However, the correlation was high (0.90 at both time points) when we restricted our analysis to significant DEGs based on an FDR cut-off value of 0.10 (Fig. 3D and E), indicating that these toxicants caused similar changes in many genes involved in liver metabolism.

Overall, we identified 227 genes in the liver that significantly changed at the 5-h time point in response to both BB and APAP exposure compared to controls (Supplementary Table S2). The majority of these genes encode proteins associated with metabolic pathways, such as those of lipid and amino acid metabolism, as well as several cancer pathways. Of the 227 genes, 29 and 18 were up- and down-regulated, respectively, with more than a 2-fold change in expression levels. This list included a diverse set of genes in several pathways, such as those of the solute carrier family (*Scl25a15* and *Scl25a32*), as well as those involved in pyrimidine (*Upp2*), amino acid (*Got1* and *Aacs*), and lipid metabolism (*Etnppl*). Similarly, at the 10-h time point, we identified 831 liver genes that significantly changed in response to both BB and APAP. Here, the contribution of genes associated with metabolic and signaling pathways significantly increased, indicating continued cellular adjustments following toxicant exposure. Compared to the 5-h time point, the number of common genes at 10 h that were up-and down-regulated with more than a 2-fold change increased to 45 (from 29) and 54 (from 18), respectively. Interestingly, although several new genes significantly changed, several top-ranked genes at the 5-h time point remained significantly changed even at the 10-h time point. Of the genes commonly activated by BB and APAP, *Hmox1* was the top-ranked upregulated gene, whereas *Adamts7* was the highest-ranked down-regulated gene. *Hmox1* plays a major role in redox regulation and the hepatic response to oxidative stress, whereas *Adamts7* is associated with tissue morphogenesis, pathophysiological remodeling, and in vascular biology (Bauer and Bauer, 2002; Kelwick et al., 2015; Origassa and Camara, 2013). Supplementary Table S2 shows a complete list of significant DEGs common to both toxicants.

3.3. Changes in absolute fluxes of central carbon metabolism

One of the major functions of the liver is to store glucose as glycogen under sated conditions and to synthesize it under fasted conditions to maintain blood glucose levels. Using MFA, we measured major metabolic fluxes in the liver glucose production pathway 10 h after administration of BB or APAP. Overall, MFA captured the major metabolic fluxes induced by either BB or APAP administration, with some differences in the pattern of fluxes for the two drugs (Fig. 4A). Compared to controls, rats given a single dose of APAP (2 g/kg) showed significant elevations in pyruvate cycling and reductions in glycogenolysis, while other enzymes in the pathway remained unchanged. In contrast, we saw no such differences between BB-treated and control animals, indicating that the two toxicants differed somewhat in how they perturbed central carbon metabolism in the liver (Fig. 4A).

3.4. Global metabolite changes in accessible biofluids

Global metabolic profiling analysis of plasma and urine samples revealed significant changes in a number of metabolites at 5 and 10 h after administration of either BB or APAP. Specifically, compared to 569 and 538 metabolites detected in the APAP study (Pannala et al., 2019), we identified 735 and 732 metabolites in plasma and urine, respectively, for the BB study. Based on an FDR cut-off value of 0.1, 446 (Fig. 4B) and 428 (Fig. 4D) metabolites significantly changed (approximately 60 %) in the plasma at 5 and 10 h, respectively, after BB administration (Supplementary Table S3). Interestingly, the trend was similar for metabolite changes in the urine, with approximately 500 (68 %) metabolites significantly changing at both time points (Fig. 4C and E, Supplementary Table S4). In contrast, for the APAP study, of the total number of metabolites detected in plasma, approximately 40 % and 30 % significantly changed relative to their controls at 5 and 10 h, respectively. These numbers were further reduced in the urine, with 20 % significantly changing at both time points (Pannala et al., 2019). These

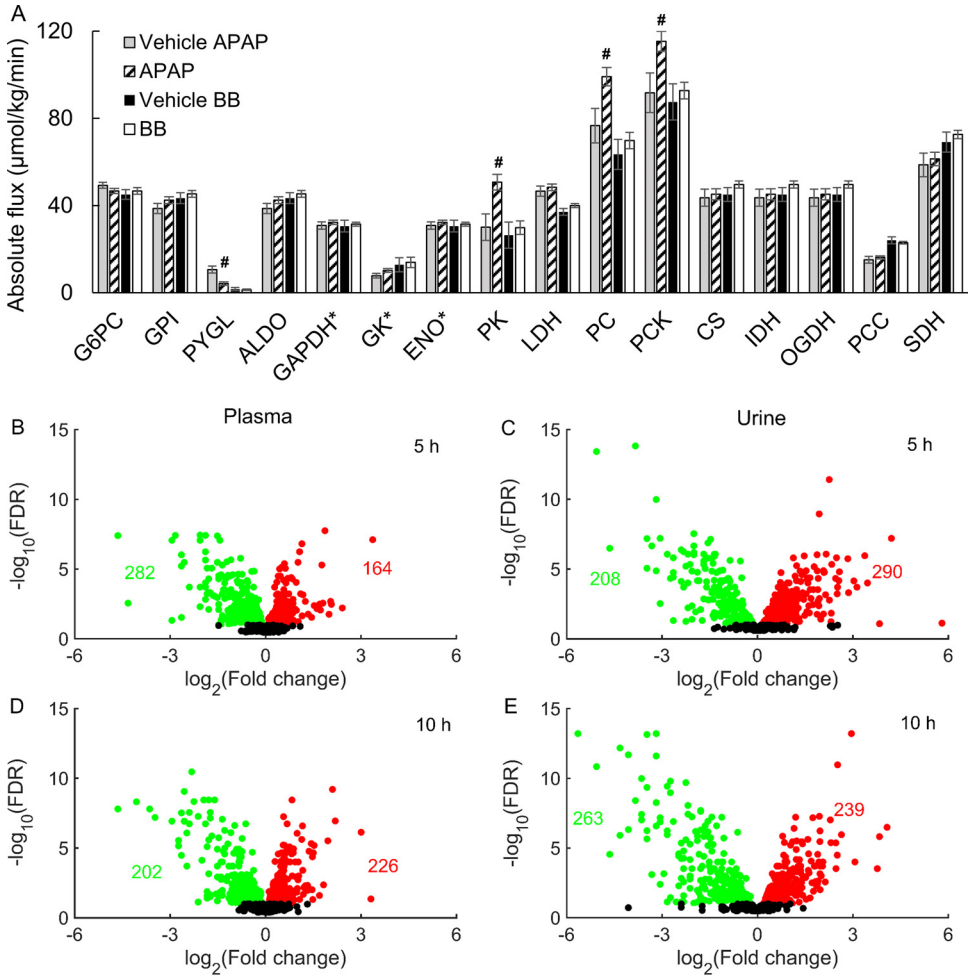

Fig. 4. Absolute hepatic flux changes induced by acetaminophen (APAP) and bromobenzene (BB) in the glucose production pathway and volcano plots of global changes in plasma and urine metabolites induced by BB. A) Bar graphs of flux measurements calculated from metabolic flux analysis 10 h after treatment with either APAP (striped bars) or BB (white bars) compared to their vehicle groups (grey or black bars, respectively). Abbreviations: ALDO, aldolase; CS, citrate synthase; ENO, enolase; GADPH, glyceraldehyde-3-phosphate dehydrogenase; GLCinf, [6,6]-$^{2}H_2$ glucose infusion; GK, glycerol kinase; GPI, D-glucose-6-phosphate isomerase; G6PC, D-glucose-6-phosphatase; IDH, isocitrate dehydrogenase; LDH, lactate dehydrogenase; OGDH, oxoglutarate dehydrogenase; PC, pyruvate carboxylase; PCC, propionyl-CoA carboxylase; PCK, phosphoenolpyruvate carboxykinase; PK, pyruvate kinase; PYGL, glycogen phosphorylase; and SDH, succinate dehydrogenase (#$p < 0.05$, *value in Hexose units). Logarithmic fold changes in metabolites induced by bromobenzene (relative to those induced by vehicle) are plotted against false discovery rates (FDRs) in the plasma after 5 h (B) and 10 h (D) and in the urine after 5 h (C) and 10 h (E). Red and green dots indicate metabolites showing significant (FDR < 0.1) increases and decreases, respectively. Black dots represent metabolites showing no significant change. In each panel, the total numbers of metabolites showing significant increases and decreases are indicated by the corresponding colors. (For interpretation of the references to color in this figure legend, the reader is referred to the web version of this article.)

results indicate that although APAP induced higher numbers of significant DEGs in the liver, these alterations may not translate into measurable changes in metabolite levels in accessible biofluids.

Analyses to identify common changes in the plasma metabolite alterations between the two studies revealed that, the similarity was greater between different time points for the same chemical than it was for different chemicals at the same time point (Fig. 5A). When we compared the two chemicals, however, the changes observed at 10 h were more closely related than were those observed at 5 h (Fig. 5A). The correlation between the two chemicals increased when we restricted our analysis to only significantly altered metabolites based on an FDR cut-off value of 0.1 (Fig. 5B at 5 h and 5C at 10 h). We observed a similar trend for metabolites that changed in the urine, where the data at the 5- and 10-h time points for each toxicant clustered together (Fig. 5D). However, the correlations between the significantly changed metabolites in the urine were lower than those in the plasma (Fig. 5E and F). Overall, our analysis revealed that the metabolite changes were better correlated in the plasma (r = 0.61 and r = 0.57) than in the

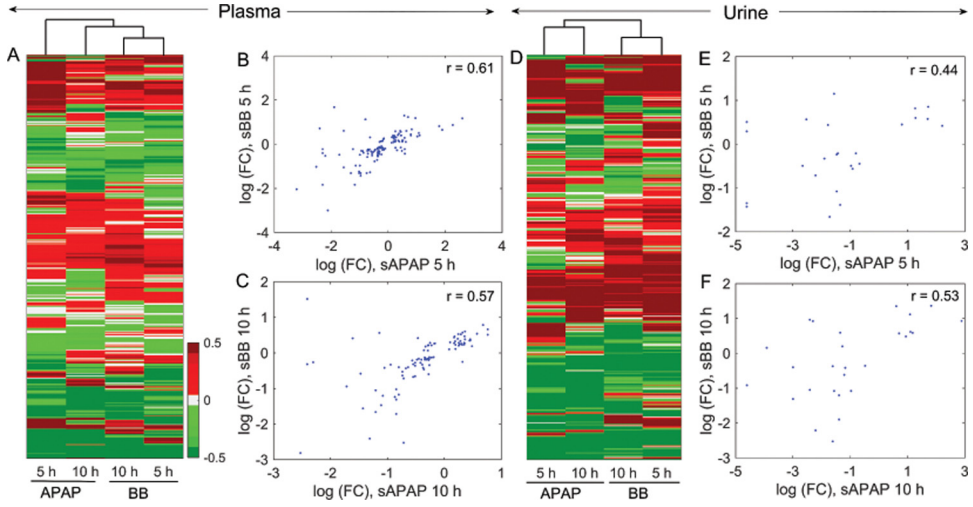

Fig. 5. Hierarchical clustering and correlation analyses of common metabolites detected in the plasma and urine after exposure to bromobenzene (BB) or acetaminophen (APAP). Clustering analysis of all common metabolites (fold changes relative to controls) in the plasma (A) and urine (D) at 5 or 10 h after BB or APAP exposure. Red and green bars indicate elevated and decreased metabolites, respectively; grey bars indicate unchanged metabolites. Correlations between the logarithmic fold changes of common metabolites significantly altered [false discover rate (FDR) < 0.1)] by BB and those significantly altered by APAP at 5 or 10 h after exposure in the plasma (B and C, respectively) and in the urine (E and F, respectively). (For interpretation of the references to color in this figure legend, the reader is referred to the web version of this article.)

urine (r = 0.44 and r = 0.53) at both time points.

We identified 121 plasma metabolites that changed significantly in both studies at 5 h (Supplementary Table S5). A majority of these metabolites belonged to the lipid, amino acid, and nucleotide metabolism pathways, among others. In particular, several metabolites of branched chain amino acids (BCAAs), such as N-acetylisoleucine, N-acetylleucine, and N-acetylvaline, as well as several metabolites involved in lipid metabolism, such as 11-dehydrocorticosterone, docosapentaenoate, margarate, corticosterone, and mead acid, increased significantly in both studies. In contrast, several sulfated metabolites, such as 3-(3-hydroxyphenyl)propionate sulfate, p-cresol sulfate, and daidzein sulfate, decreased significantly in both studies. Similarly, at 10 h, 96 plasma metabolites changed significantly in both studies. Consistent with the changes observed at 5 h, several metabolites in the BCAA and nucleotide metabolism pathways increased, whereas several sulfated metabolites decreased, indicating persistent perturbations in these pathways due to toxicant exposure. In addition, several metabolites in the sphingomyelin metabolism pathway increased significantly. In contrast to the changes observed in the plasma, few urine metabolites changed in both studies. Supplementary Table S5 shows a complete list of metabolites that significantly changed in both studies.

3.5. Multi-tissue GSMs predict metabolites associated with mechanisms of toxicity

The global analyses revealed several genes and metabolites that significantly changed in both studies, along with toxicant-specific changes. However, these analyses do not provide any mechanistic explanation for the observed changes. Although gene-expression changes are one of the major drivers, metabolites in biofluids can change due to several factors, including contributions from all organs involved in their systemic circulation. Therefore, we used a multi-tissue GSM (Fig. 6A) to integrate the high-throughput data and simulated the changes in plasma and urine metabolites based on concomitantly measured gene-expression changes in liver and kidney tissues. Fig. 6B shows a summary of the significant alterations that mapped to the GSM from the BB study. Approximately 1700 and 1800 metabolic genes from the liver and kidney, respectively, mapped to the GSM at both time points. Among the former (i.e., the mapped genes in the liver), 116 and 381 changed significantly at 5 and 10 h, respectively (Fig. 6B), indicating that these genes could potentially drive the metabolite changes in the plasma and urine. Similarly, of the total metabolites detected in the global profiling analyses, only ~30 % mapped to the GSM, with nearly half changing significantly (Fig. 6C). The coverage was similar for the APAP study, although the total numbers of metabolites detected in the plasma and urine were smaller (Pannala et al., 2019).

We conducted systems-level analyses to assess the predictions of the multi-tissue GSM against the changes observed in the global metabolic profiling analysis (Tables S3 and S4), and identify metabolites that are causally related to the gene-expression changes. The multi-tissue GSM correctly evaluated the direction of change (an increase or decrease) for approximately 60 % of the mapped metabolites that significantly changed in both the plasma and urine 10 h after BB exposure (Fig. 6C, Supplementary Table S6). In contrast, when we provided the GSM with random gene-expression changes as the inputs, it evaluated the direction of change correctly for only about 30 % of the same metabolites. Similarly, at 5 h, the model predicted the direction of change for approximately 39 % and 58 % of the metabolites that significantly changed in the plasma and urine, respectively, showing little difference from the condition where we used random gene-expression changes as inputs (Fig. 6C, Supplementary Table S6). The systems-level analysis results for BB resembled the results obtained with APAP, for which the GSM correctly evaluated 66 % of the plasma metabolites associated with the gene-expression changes at 10 h but fewer at 5 h (Pannala et al., 2019). These results for APAP and BB demonstrate that many of the metabolite changes were correlated with gene-expression changes in the liver at 10 h, where the number of genes and their magnitude of change were significant. Furthermore, our model assessments were similar with or without the inclusion of changes in kidney gene expression, suggesting that most of the observed changes were due to toxicant-induced changes in liver metabolism.

3.6. Metabolites associated with mechanisms of liver toxicity

To ascertain possible causality between the gene-expression changes in the liver and the metabolite changes in biofluids, we focused on genes associated with metabolic pathways and processes. Fig. 7 shows genes that changed significantly in both studies, and which are involved in the metabolism of lipids, carbohydrates, amino acids, nucleotides, cofactors or vitamins, and xenobiotics. In particular, a majority of the subordinate pathways in lipid metabolism changed similarly for BB and APAP at both time points. One exception was the pathway for

A

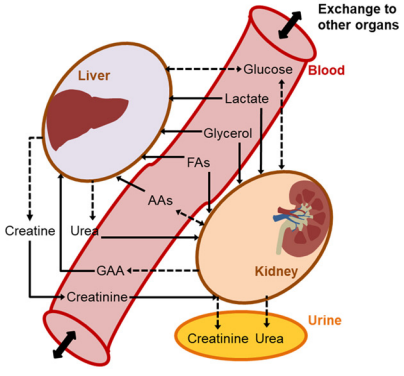

B

Significant metabolic alterations mapped to multi-tissue model in the BB study (FDR < 0.1)

Genes	Liver		Kidney	
Time (h)	Increased	Decreased	Increased	Decreased
5	57	59	5	5
10	160	221	92	29
Metabolites	**Plasma**		**Urine**	
Time (h)	Increased	Decreased	Increased	Decreased
5	60	72	114	29
10	85	57	85	48

C

Summary of the multi-tissue model predictions for the BB study

Sample	Time (h)	Metabolites mapped to the model	Significantly changed metabolites	Model predictions based on gene-expression data	
				Random (%)	Actual (%)
Plasma	5	238	109	37	39
	10	238	121	34	62
Urine	5	219	131	50	58
	10	219	121	30	61

Fig. 6. Predictions of metabolite changes driven by gene-expression changes using multi-tissue genome-scale models (GSMs). A) Schematic of a rat multi-tissue GSM that captures inter-organ connectivity between the liver and kidneys via blood and urine compartments. Solid, dashed, and dashed bidirectional arrows denote the movements of molecules between compartments (uptake, secretion, and mutual exchange, respectively). These relationships served as constraints for the kidney and liver to simulate the metabolite alterations. Abbreviations: AAs, amino acids; FAs, fatty acids; and GAA, guanidinoacetic acid. B) Summary of significant gene-expression changes in the liver and kidney, and metabolite alterations in the plasma and urine mapped to the multi-tissue GSM. C) Summary of model predictions for metabolites in the plasma and urine based on the integration of gene-expression changes in the liver and kidneys.

Main pathway	Subordinate pathway	Bromobenzene				Acetaminophen			
		5 h		10 h		5 h		10 h	
		Genes	z-score	Genes	z-score	Genes	z-score	Genes	z-score
Lipid metabolism	Fatty acid metabolism			17	-1.90			11	-1.17
	Steroid biosynthesis	7	-2.69	9	-3.84			9	-3.74
	Steroid hormone biosynthesis	7	0.08	12	-1.36			26	-4.24
	Fatty acid degradation			12	-0.11			15	-0.42
	Fatty acid elongation			8	0.01				
	Glycerolipid metabolism			14	2.52	8	1.04	17	-0.01
	Glycerophospholipid metabolism	7	1.27	17	2.06	14	1.35	19	0.88
	Biosynthesis of unsaturated fatty acids	4	-2.19	11	-1.34				
	Sphingolipid metabolism					8	0.11		
Carbohydrate metabolism	Carbon metabolism	5	1.70	22	-1.16	11	0.46	38	1.80
	Pyruvate metabolism			12	-2.15			16	-0.75
	Glyoxylate and dicarboxylate metabolism			10	-2.15			11	-1.37
	Amino sugar and nucleotide sugar metabolism			11	-1.58	11	-1.29	12	-0.49
	Fructose and mannose metabolism			8	1.05	7	0.62		
	Glycolysis / Gluconeogenesis			11	-1.72			17	0.31
	Citrate cycle							12	1.50
Amino-acid metabolism	Cysteine and methionine metabolism	5	2.87	12	1.37	7	1.30	16	1.92
	Arginine and proline metabolism			11	0.83			11	0.62
	Tryptophan metabolism			9	-0.90			14	-3.51
	Biosynthesis of amino acids							23	3.65
	Glycine, serine and threonine metabolism					7	0.54	16	1.69
	Glutathione metabolism							14	-0.01
Nucleotide metabolism	Purine metabolism							33	-0.15
	Pyrimidine metabolism							24	-1.03
Cofactors and vitamins	Retinol metabolism							21	-2.97
	Nicotinate and nicotinamide metabolism							11	-1.91
Xenobiotic metabolism	Metabolism of xenobiotics by cytochrome P450							17	-1.29
	Drug metabolism - cytochrome P450							13	-2.55

Fig. 7. Summary of significant metabolic pathways identified using gene-enrichment analysis for bromobenzene and acetaminophen, based on gene-expression changes in the liver mapped to the multi-tissue GSM. Metabolic pathways perturbed significantly for both toxicants are shaded in grey, whereas those perturbed selectively are shaded in yellow (based on z-scores from the AFC method). (For interpretation of the references to color in this figure legend, the reader is referred to the web version of this article.)

biosynthesis of unsaturated fatty acids, in which many of the involved genes showed marked downregulation only for BB exposure. Genes in the glycolysis- and citrate cycle-related pathways of carbohydrate metabolism were differentially regulated for the two toxicants. Similarly, amino acid, cofactor/vitamin, and nucleotide metabolism also markedly differed between the two toxicants. For example, several genes in the nucleotide and cofactor/vitamin metabolism pathways were significantly downregulated only by APAP. Similarly, many genes in amino acid biosynthesis pathways showed substantial upregulation only after APAP exposure. In particular, only APAP exposure led to upregulation of several genes in the glycine, serine, and threonine/glutathione metabolism pathways, indicating the extensive utilization of GSH pools for toxicant clearance.

3.7. Metabolites in highly enriched pathways as indicators of liver toxicity

Based on the predictions of the multi-tissue GSM and pathway enrichment analysis, we determined highly enriched pathways in liver metabolism and compiled a plausible panel of significantly altered plasma metabolites strongly correlated with changes in gene expression. Tables 1 and 2 show lists of these metabolites in the plasma, which the multi-tissue model predicted correctly for both APAP and BB studies. In particular, several plasma metabolites showed opposite responses in the two studies (Table 1), reflecting the differences observed in the gene-expression changes in amino acid metabolism. For example, several metabolites in the arginine and proline metabolism pathways significantly decreased only after APAP exposure. Similarly, metabolites in the phenylalanine/tyrosine, tryptophan, and lysine metabolism pathways only increased after BB exposure. Furthermore, metabolites in the glycine, serine, and threonine metabolism pathway increased after BB exposure but decreased after APAP exposure, suggesting their potential to serve as toxicant-specific markers. In contrast to the changes in amino acid metabolism, plasma metabolite changes in lipid metabolism showed notable similarities (Table 2). For example, both toxicants showed increases in stearate and oleate, which are metabolites involved in fatty acid metabolism, as well as metabolites related to choline and sphingosine in phospholipid metabolism. Similarly, both toxicants led to reductions of several metabolites involved in bile-acid metabolism, including glycocholate, chenodeoxycholate, hyodeoxycholate, hyocholate, and β-muricholate. These results suggest that the mechanistic pathways impacted similarly by both toxicants, as well as the metabolites within them, should be closely scrutinized to identify potential indicators of liver toxicity.

4. Discussion

The prediction and early diagnosis of liver injuries due to drugs and environmental factors is critical for ensuring the best possible management of patients, and for preventing injuries from progressing to acute liver failure. Accordingly, there is a need to establish non-invasive markers of liver injuries and elucidate the mechanisms underlying disease progression. In the present study, we compared the transcriptome and metabolome profiles of rats treated with one of two classical hepatotoxicants (APAP and BB) and those of healthy controls under identical experimental conditions. We combined the global profiling analysis with a multi-tissue GSM and elucidated pathways critical for liver metabolism, which undergo toxicant-mediated perturbations as early as 5 h after exposure. Our findings included a marked correlation between genes in the liver and metabolites in biofluids, which were significantly altered in toxicant-treated rats when compared with healthy controls. Furthermore, GSM-based analysis led to the identification of several important metabolic pathways in liver metabolism that undergo injury-specific alterations shortly after toxicant exposure. Identification of these injury-specific metabolic pathways, in turn, allowed us to identify several new metabolites in the plasma and urine with the potential to indicate early perturbations in liver metabolism and, thereby, detect an impending liver injury. These results demonstrate the utility of a mechanistic approach to systematically probe injury-specific alterations in organ metabolism, which could provide an effective means to identify candidate markers of liver injuries in the future.

This study represents one of the first toxicogenomics studies to analyze acute hepatotoxicity at the transcriptomic level using RNA-sequencing and global metabolite profiling analysis in accessible

Table 1
Significantly altered plasma metabolites in amino-acid pathways based on model predictions at 5 and 10 h after exposure to bromobenzene or acetaminophen. Metabolites in bold indicate those that changed significantly (FDR < 0.1) in both studies.

Metabolic pathway	Metabolite	log_2(fold change)			
		Bromobenzene		Acetaminophen	
		5 h	10 h	5 h	10 h
Arginine and proline	Ornithine	0.20			
	Proline			−0.20	−0.34
	Citrulline				−0.20
	Argininosuccinate				−0.36
	Ornithine				−0.64
	trans-4-hydroxyproline			−0.36	−0.71
	Guanidinoacetate				−0.80
	5-oxoproline	0.17	0.23		
	Creatine	**0.16**	**0.37**		**0.43**
	Spermidine		**0.95**	**−0.81**	**1.10**
	5-methylthioadenosine		0.27		
	Putrescine		0.28		
	2-hydroxybutyrate		0.27		
Glycine, serine, and threonine	**Glycine**	**0.31**	**0.41**	**−0.25**	**−0.36**
	Sarcosine	**0.20**	**0.36**	**−0.30**	
	Serine	**0.37**	**0.31**	**−0.22**	**−0.42**
	Glycerate			−0.22	−0.30
	Dimethylglycine				0.36
Valine, leucine, and isoleucine	3-methyl-2-oxobutyrate		0.30		
	3-hydroxyisobutyrate	0.57	1.02		
Histidine	Urocanate		0.40		
	Methylimidazoleacetic acid			−1.10	−1.03
Alanine, aspartate, and glutamate	**Asparagine**	**0.19**	**0.31**	**−0.36**	**−0.40**
	Glutamine		0.13		
	Alanine			−0.14	−0.14
	Aspartate				−0.38
	Glutamate				−0.43
	1-pyrroline-5-carboxylate			−0.67	−0.64
	N-acetylaspartate			−0.43	
Phenylalanine and tyrosine	Phenylacetate		1.95		
Tryptophan	Serotonin	0.54	3.31		
	Picolinic acid		2.10		
	Anthranilate	0.57	1.04		
Lysine	2-oxoadipate		0.45		

biofluids. We integrated the transcriptomic and metabolomic data with a GSM to increase the sensitivity of detecting hepatotoxicity and evaluating relationships between gene-expression and metabolite changes within and across different hepatotoxicants. We selected the dose and time points for toxicant exposures so that they elicited no immediate response but showed marked increases in the levels of current clinical markers as time progressed. Therefore, our study design provided a way to probe early molecular perturbations in liver metabolism before they led to maximal toxicity, as measured by conventional methods.

Consistent with the known hepatotoxic effects of BB and APAP, our analysis of global changes in genes at the tissue level, together with the corresponding alterations in biofluids, indicated that these toxicants primarily affected the liver and not the kidneys. Importantly, despite differences in the total number of significant DEGs in the liver between the two studies, the correlations between the DEGs were high at both time points. Hierarchical clustering analysis revealed that the gene-expression changes for the 10-h groups were more closely clustered than were those for the 5-h groups when we compared changes between the two chemicals. Our results concur with a previous microarray study in which similar analyses were performed with a large number of hepatotoxicants, including BB and APAP (Minami et al., 2005). Although our study differed in experimental setup, dose, time of assessment after exposure, and platform of detection, we identified several common genes that were significantly up- or down-regulated similarly across conditions and toxicants (Supplementary Table S2). For example, the genes for heme oxygenase (*Hmox1*), thioredoxin reductase 1 (*Txnrd1*), activating transcription factor (*Atf*), cathepsin L (*ctsl*), and DNA-damage-inducible transcript 1 (*Gadd45a*), were commonly altered by different hepatotoxicants across conditions, suggesting a common mechanism of toxicity. In particular, we identified metabolic changes as early as 10 h after toxicant exposure, which persisted long after liver injury became evident (48 h after toxicant exposure), as noted in a previous study (Minami et al., 2005). The results demonstrate that, by using advanced techniques, we can measure metabolic perturbations well before injury occurs.

Unlike gene-expression changes in tissues, global metabolic profiling allows non-invasive measurement of hundreds of different metabolites in accessible biofluids using sensitive and specific methods. Metabolomics has been used to identify markers for disease diagnosis, disease prognosis, and toxicity assessment, as well as to gain a greater pathophysiological understanding of the disease (Lin et al., 2011). We identified significant changes in several plasma and urine metabolites induced by BB, many of which were also induced by APAP. Some metabolites identified in the fatty acid and amino acid metabolism pathways, among others, were consistent with results previously reported for APAP (Chen et al., 2009; Kumar et al., 2012). Similarly, a global profiling analysis for BB revealed a large number of plasma and urine metabolites that significantly changed at both time points. Many of these metabolite changes in pathways related to glycolysis, and the metabolism of GSH, amino acids, and lipids, were consistent with previous observations (Heijne et al., 2005; Waters et al., 2006). Overall, the number of common metabolites that changed significantly in the plasma was higher than that in the urine for both toxicants. Thus, plasma metabolites should be probed in future studies to identify new indicators of liver toxicity (Fig. 5 and Supplementary Table S5).

Any metabolite discovered in a global metabolic analysis could

Table 2
Significantly altered plasma metabolites in lipid-metabolism pathways based on model predictions at 5 and 10 h after exposure to bromobenzene or acetaminophen.

Metabolic pathway	Metabolite	log_2(fold change)			
		Bromobenzene		Acetaminophen	
		5 h	10 h	5 h	10 h
Fatty acids	Arachidonate	0.80	0.34		
	Palmitate		0.50		
	4-hydroxy-2-oxoglutarate		0.46		
	Stearate	**0.23**	**0.50**	**0.71**	
	Oleate		**0.45**		**0.86**
	Palmitoylcarnitine	0.59	0.67		
	Myristic acid		0.34		
	Linolenate		0.44		
	EPA		0.98		
	DHA		0.61		
	Palmitolate	0.82	0.47		
	DPA		0.60		
	16-hydroxupalmitate		0.45		
	O-acetylcarnitine		0.32		
	Oleoylcarnitine	0.33	0.54		
	Stearoylcarnitine	0.51	0.83		
	Stearidonic acid	0.52			
	Mead acid	0.97			
	Caproate	−0.49	−0.57		
	Azelate	−1.02	−0.37		
	Behenic acid	−1.78			
	Butyrate		−0.39		
Phospholipids, ketone, and sphingolipids	**Choline**		**0.16**	**0.30**	**0.29**
	Ethanolamine phosphate	0.16			
	(R)-3-hydroxybutanoate	0.84	1.50		
	Acetoacetate	0.86	0.47		
	Sphingosine		**1.35**		**0.62**
	Sphingosine-1-phosphate		**0.41**		**0.37**
	Stearoyl sphingomyelin		**0.78**	**0.32**	**0.83**
	Sphinganine-1-phosphate	0.79	1.32		
Bile acids	Cholate		−1.05		
	Glycocholate		**−0.64**	**−2.25**	
	Chenodeoxycholate		**−1.43**	**−1.10**	**−1.64**
	Deoxycholic acid		−0.94		
	Glycodeoxycholate		−1.35		
	Glycochenodeoxycholate		−1.15		
	Ursodeoxycholate		−0.81		
	Murideoxycholic acid		−1.50		
	Hyodeoxycholate		**−1.78**	**−2.94**	
	α-muricholate		−1.00		
	Hyocholate		**−1.83**	**−3.64**	
	β-muricholate		**−0.76**	**−1.84**	
	Glycohyodeoxycholate		−1.73		

potentially be a new marker. However, to fully explore the capability of such a metabolite, we need to establish the causality between its change in response to toxicant exposure and the ensuing injury in the organ of interest. Therefore, of the hundreds of metabolites that change significantly in global metabolic profiling, we need to identify those whose alterations causally linked to the toxicant's mechanism of action. Using a multi-tissue GSM, we identified several metabolites in the plasma and urine, whose alterations were driven by gene-expression changes that were commonly induced in the liver by both toxicants (Supplementary Table S5). By mapping global gene-expression changes to the GSM, we identified several metabolic genes that participate in various pathways crucial for liver metabolism (Fig. 7). Fig. 8 summarizes key similarities and differences in the metabolic pathways perturbed by BB and APAP. For example, some genes changed similarly for both toxicants (i.e., in the glycolysis, TCA cycle, and fatty acid metabolism pathways), whereas several genes involved in glycerophospholipid metabolism significantly changed only in response to APAP or BB (Fig. 8, top panels). Specifically, these genes were either up- or down-regulated only by BB, indicating differences in lipid accumulation between BB toxicity (AbdulHameed et al., 2019; Sahini et al., 2014) and APAP toxicity, presumably due to impaired mitochondrial β-oxidation.

One of the common mechanisms through which the liver detoxifies BB and APAP is the conjugation of GSH, a molecule that acts as a free radical scavenger (Benedetti et al., 1986; Nelson, 1990; Ramachandran and Jaeschke, 2018; Thor and Orrenius, 1980). However, an overdose of BB or APAP depletes GSH pools, leading to an excess of free radical molecules and, hence, injury. Therefore, cells must actively replenish their GSH stores by resynthesizing GSH using amino acids (e.g., cysteine, glutamate, and glycine) as precursors. Several genes involved in the metabolism of arginine and proline, as well as cysteine and methionine, changed similarly for both BB and APAP, but not those involved in the metabolism of serine, glycine, and proline (Fig. 8, bottom panels). In contrast, APAP induced upregulation of genes involved in the synthesis of glycine, which coincided with significant decreases in plasma glycine and serine concentrations. These gene and metabolite alterations involved in the metabolism of serine, glycine, and proline suggest that, compared to BB exposure, APAP exposure leads to marked depletion of GSH stores, which results in the upregulation of compensatory synthesis pathways for GSH replenishment. Overall, these results show that BB and APAP exposure, despite commonly inducing changes in several genes involved in various metabolic pathways, can lead to different metabolite changes in accessible biofluids.

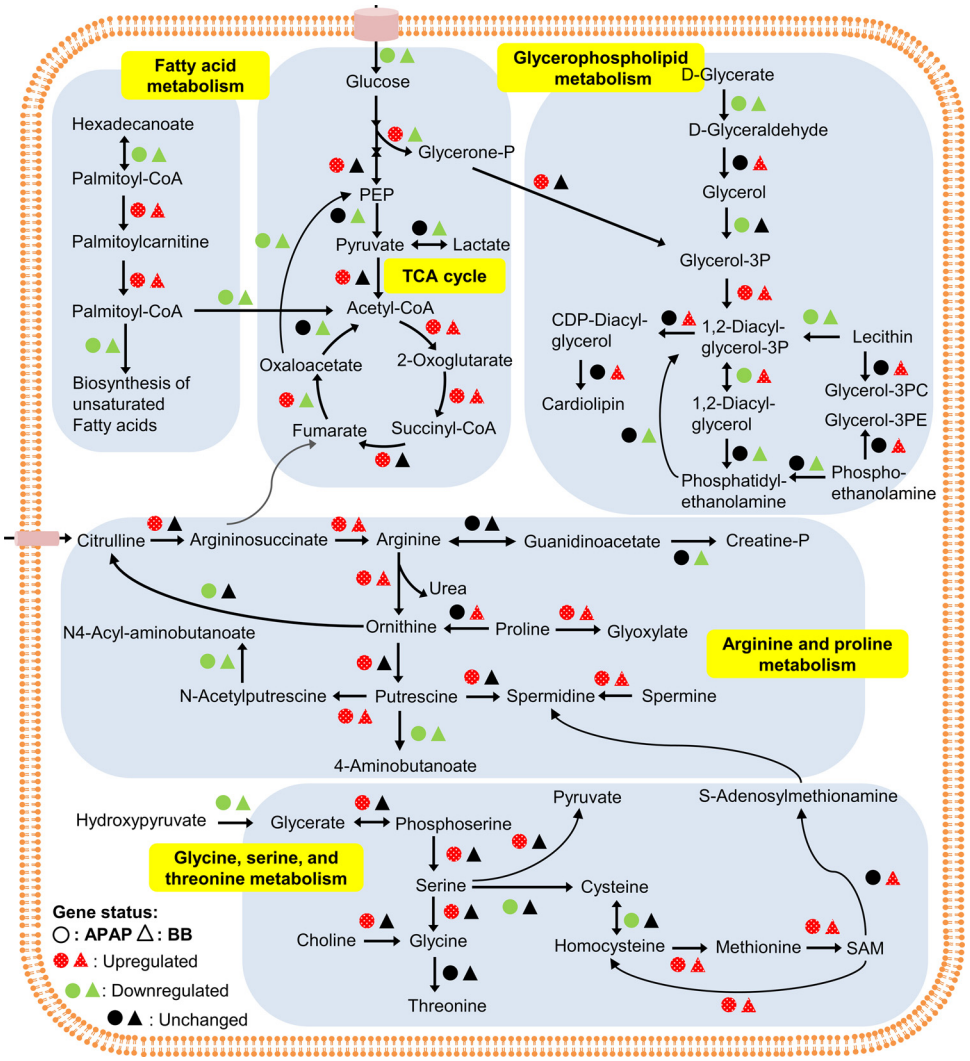

Fig. 8. Schematic representation summarizing bromobenzene (BB)- and acetaminophen (APAP)-induced perturbations of various metabolic pathways in the liver of the rat. The significantly enriched liver-metabolism pathways are based on genes significantly altered 10 h after exposure to either BB or APAP. Arrows indicate the directionality of reactions. The perturbation of a gene responsible for a reaction, induced by exposure to BB (triangles) or APAP (circles), is shown in red [significantly upregulated, false discovery rate (FDR) < 0.1], green (significantly downregulated, FDR < 0.1), or black (unchanged). (For interpretation of the references to color in this figure legend, the reader is referred to the web version of this article.)

Integration of the transcriptomic data together with the network model allowed us to decipher the metabolites in the plasma and urine whose alterations strongly correlated with changes in gene expression. We identified approximately 60 % of the significantly changed metabolites driven by gene-expression changes in both studies (Supplementary Table S6). Several plasma metabolites related to lipid metabolism changed similarly in both studies, suggesting common mechanisms of toxicity. In particular, several metabolites in the bile-acid pathway, which are more specific to the liver than to the kidneys, significantly decreased in the plasma at one or more time points in both studies (Table 2). Interestingly, serum bile-acid profiles have previously been proposed as markers of liver injury and disease in humans (Luo et al., 2018), and have been investigated as novel candidate markers of drug-induced liver injuries (Ma et al., 2019). Overall, our model predictions provided a set of metabolites strongly correlated with gene-expression changes, which can be further used to investigate mechanism-based indicators of liver injury (Tables 1 and 2).

In summary, we systematically evaluated hepatotoxicant-induced alterations in the endogenous metabolism of rats and identified global changes in liver and kidney genes, as well as plasma and urine metabolites. We identified significant correlations between gene-expression changes in the liver induced by two hepatotoxicants, BB and APAP. However, the changes in metabolites in accessible biofluids induced by BB and APAP did not correlate to the same extent as did the changes in gene expression in the liver. Using a multi-tissue GSM, we identified injury-specific pathways and metabolites within them whose alterations were causally related to the mechanism of toxicity. Thus, we identified several toxicant-specific and common metabolites involved in amino acid and lipid metabolism, which could serve as potential indicators of toxicant-induced liver damage. Our results demonstrate that GSMs can serve as useful tools to integrate high-throughput data from multiple toxicants, elucidate the underlying mechanisms of chemical-induced toxicity, and suggest potential strategies to identify new indicators of organ injury.

Author contributions

VRP carried out the RNA-sequencing analysis, integrated the high-throughput data, developed the computational model, and wrote the initial draft of the manuscript. SKE performed all of the animal studies, including catheterization surgeries. MR performed the metabolic flux calculations. IT performed the mass spectrometry analysis of plasma samples obtained from stable isotope infusions. TPO collected and analyzed all of the blood and urine samples. RLP and CS contributed to the extraction of RNA from tissue and its purification. JR conceived and supervised the study, and helped edit the manuscript. TO helped edit the manuscript. MS conceived the study, supervised and carried out the experiments on rats to generate the raw data, and helped write the manuscript. JDY conceived the study, provided supervision, performed metabolic flux analysis, and helped write the manuscript. AW conceived and supervised the study, analyzed the data, and helped edit and write the final manuscript.

Declaration of Competing Interest

The authors declare that they have no known competing financial interests or personal relationships that could have appeared to influence the work reported in this paper.

Acknowledgements

The authors were supported by the U.S. Army Medical Research and Development Command, Ft. Detrick, MD, as part of the U.S. Army's Network Science Initiative. Dr. Jamey Young was supported under Contract No. W81XWH-14-C-0058. VANTAGE was supported in part by a Clinical and Translational Science Award (CSTA) Grant (5UL1 RR024975-03), the Vanderbilt Ingram Cancer Center (P30 CA68485), the Vanderbilt Vision Center (P30 EY08126), and NIH/NCRR (G20 RR030956). The Vanderbilt University Medical Center VANTAGE Core provided the genome-wide RNA-sequencing data; Metabolon Inc. provided the global metabolic profiling data and some technical assistance for this work. The opinions and assertions contained herein are the private views of the authors and are not to be construed as official or as reflecting the views of the U.S. Army, the U.S. Department of Defense, or The Henry M. Jackson Foundation for Advancement of Military Medicine, Inc. This paper has been approved for public release with unlimited distribution.

Appendix A. Supplementary data

Supplementary material related to this article can be found, in the online version, at doi:https://doi.org/10.1016/j.tox.2020.152493.

References

AbdulHameed, M.D.M., Pannala, V.R., Wallqvist, A., 2019. Mining public toxicogenomic data reveals insights and challenges in delineating liver steatosis adverse outcome pathways. Front. Genet. 10, 1007.
Alfirevic, A., Pirmohamed, M., 2012. Predictive genetic testing for drug-induced liver injury: considerations of clinical utility. Clin. Pharmacol. Ther. 92, 376–380.
Antoine, D.J., Jenkins, R.E., Dear, J.W., Williams, D.P., McGill, M.R., Sharpe, M.R., Craig, D.G., Simpson, K.J., Jaeschke, H., Park, B.K., 2012. Molecular forms of HMGB1 and keratin-18 as mechanistic biomarkers for mode of cell death and prognosis during clinical acetaminophen hepatotoxicity. J. Hepatol. 56, 1070–1079.
Antoine, D.J., Dear, J.W., Lewis, P.S., Platt, V., Coyle, J., Masson, M., Thanacoody, R.H., Gray, A.J., Webb, D.J., Moggs, J.G., Bateman, D.N., Goldring, C.E., Park, B.K., 2013. Mechanistic biomarkers provide early and sensitive detection of acetaminophen-induced acute liver injury at first presentation to hospital. Hepatology 58, 777–787.
Antoniewicz, M.R., Kelleher, J.K., Stephanopoulos, G., 2006. Determination of confidence intervals of metabolic fluxes estimated from stable isotope measurements. Metab. Eng. 8, 324–337.
Antoniewicz, M.R., Kelleher, J.K., Stephanopoulos, G., 2011. Measuring deuterium enrichment of glucose hydrogen atoms by gas chromatography/mass spectrometry. Anal. Chem. 83, 3211–3216.
Baloni, P., Sangar, V., Yurkovich, J.T., Robinson, M., Taylor, S., Karbowski, C.M., Hamadeh, H.K., He, Y.D., Price, N.D., 2019. Genome-scale metabolic model of the rat liver predicts effects of diet restriction. Sci. Rep. 9, 9807.
Bauer, M., Bauer, I., 2002. Heme oxygenase-1: redox regulation and role in the hepatic response to oxidative stress. Antioxid. Redox Signal. 4, 749–758.
Beger, R.D., Sun, J., Schnackenberg, L.K., 2010. Metabolomics approaches for discovering biomarkers of drug-induced hepatotoxicity and nephrotoxicity. Toxicol. Appl. Pharmacol. 243, 154–166.
Bellomo, G., Orrenius, S., 1985. Altered thiol and calcium homeostasis in oxidative hepatocellular injury. Hepatology 5, 876–882.
Benedetti, A., Pompella, A., Fulceri, R., Romani, A., Comporti, M., 1986. 4-Hydroxynonenal and other aldehydes produced in the liver in vivo after bromobenzene intoxication. Toxicol. Pathol. 14, 457–461.
Blais, E.M., Rawls, K.D., Dougherty, B.V., Li, Z.I., Kolling, G.L., Ye, P., Wallqvist, A., Papin, J.A., 2017. Reconciled rat and human metabolic networks for comparative toxicogenomics and biomarker predictions. Nat. Commun. 8, 14250.
Bray, N.L., Pimentel, H., Melsted, P., Pachter, L., 2016. Near-optimal probabilistic RNA-seq quantification. Nat. Biotechnol. 34, 525–527.
Campion, S., Aubrecht, J., Boekelheide, K., Brewster, D.W., Vaidya, V.S., Anderson, L., Burt, D., Dere, E., Hwang, K., Pacheco, S., Saikumar, J., Schomaker, S., Sigman, M., Goodsaid, F., 2013. The current status of biomarkers for predicting toxicity. Expert Opin. Drug Metab. Toxicol. 9, 1391–1408.
Chen, C., Krausz, K.W., Shah, Y.M., Idle, J.R., Gonzalez, F.J., 2009. Serum metabolomics reveals irreversible inhibition of fatty acid beta-oxidation through the suppression of PPARalpha activation as a contributing mechanism of acetaminophen-induced hepatotoxicity. Chem. Res. Toxicol. 22, 699–707.
Chong, J., Soufan, O., Li, C., Caraus, I., Li, S., Bourque, G., Wishart, D.S., Xia, J., 2018. MetaboAnalyst 4.0: towards more transparent and integrative metabolomics analysis. Nucleic Acids Res. 46, W486–W494.
Cunningham, F., Achuthan, P., Akanni, W., Allen, J., Amode, M.R., Armean, I.M., Bennett, R., Bhai, J., Billis, K., Boddu, S., Cummins, C., Davidson, C., Dodiya, K.J., Gall, A., Giron, C.G., Gil, L., Grego, T., Haggerty, L., Haskell, E., Hourlier, T., Izuogu, O.G., Janacek, S.H., Juettemann, T., Kay, M., Laird, M.R., Lavidas, I., Liu, Z., Loveland, J.E., Marugan, J.C., Maurel, T., McMahon, A.C., Moore, B., Morales, J., Mudge, J.M., Nuhn, M., Ogeh, D., Parker, A., Parton, A., Patricio, M., Abdul Salam, A.I., Schmitt, B.M., Schuilenburg, H., Sheppard, D., Sparrow, H., Stapleton, E., Szuba, M., Taylor, K., Threadgold, G., Thormann, A., Vullo, A., Walts, B., Winterbottom, A., Zadissa, A., Chakiachvili, M., Frankish, A., Hunt, S.E., Kostadima, M., Langridge, N., Martin, F.J., Muffato, M., Perry, E., Ruffier, M., Staines, D.M., Trevanion, S.J., Aken, B.L., Yates, A.D., Zerbino, D.R., Flicek, P., 2019. Ensembl 2019. Nucleic Acids Res. 47, D745–D751.
Dehaven, C.D., Evans, A.M., Dai, H., Lawton, K.A., 2010. Organization of GC/MS and LC/MS metabolomics data into chemical libraries. J. Cheminform. 2, 9.
Drescher, H.K., Weiskirchen, S., Weiskirchen, R., 2019. Current status in testing for nonalcoholic fatty liver disease (NAFLD) and Nonalcoholic Steatohepatitis (NASH). Cells 8, 845.
Eguchi, A., Wree, A., Feldstein, A.E., 2014. Biomarkers of liver cell death. J. Hepatol. 60, 1063–1074.
Evans, A., Bridgewater, B., Liu, Q., Mitchell, M., Robinson, R., Dai, H., Stewart, S., DeHaven, C., Miller, L., 2014. High resolution mass spectrometry improves data quantity and quality as compared to unit mass resolution mass spectrometry in high-throughput profiling metabolomics. Metabolomics 4, 1.
Gille, C., Bolling, C., Hoppe, A., Bulik, S., Hoffmann, S., Hubner, K., Karlstadt, A., Ganeshan, R., Konig, M., Rother, K., Weidlich, M., Behre, J., Holzhutter, H.G., 2010. HepatoNet1: a comprehensive metabolic reconstruction of the human hepatocyte for the analysis of liver physiology. Mol. Syst. Biol. 6, 411.
Hasenour, C.M., Wall, M.L., Ridley, D.E., Hughey, C.C., James, F.D., Wasserman, D.H., Young, J.D., 2015. Mass spectrometry-based microassay of (2)H and (13)C plasma glucose labeling to quantify liver metabolic fluxes in vivo. Am. J. Physiol. Endocrinol. Metab. 309, E191–203.
Hatano, T., Saiki, S., Okuzumi, A., Mohney, R.P., Hattori, N., 2016. Identification of novel biomarkers for Parkinson's disease by metabolomic technologies. J Neurol Neurosurg Psychiatry 87, 295–301.
Heijne, W.H., Stierum, R.H., Slijper, M., van Bladeren, P.J., van Ommen, B., 2003. Toxicogenomics of bromobenzene hepatotoxicity: a combined transcriptomics and proteomics approach. Biochem. Pharmacol. 65, 857–875.
Heijne, W.H., Lamers, R.J., van Bladeren, P.J., Groten, J.P., van Nesselrooij, J.H., van Ommen, B., 2005. Profiles of metabolites and gene expression in rats with chemically induced hepatic necrosis. Toxicol. Pathol. 33, 425–433.
Heinloth, A.N., Boorman, G.A., Foley, J.F., Flagler, N.D., Paules, R.S., 2007. Gene expression analysis offers unique advantages to histopathology in liver biopsy evaluations. Toxicol. Pathol. 35, 276–283.
Huang, D.W., Sherman, B.T., Lempicki, R.A., 2009. Systematic and integrative analysis of large gene lists using DAVID bioinformatics resources. Nat. Protoc. 4, 44–57.
Jerby, L., Shlomi, T., Ruppin, E., 2010. Computational reconstruction of tissue-specific metabolic models: application to human liver metabolism. Mol. Syst. Biol. 6, 401.
Kaptanoglu, L., Kurt, N., Sikar, H.E., 2017. Current approach to liver traumas. Int. J. Surg. 39, 255–259.
Kelwick, R., Desanlis, I., Wheeler, G.N., Edwards, D.R., 2015. The ADAMTS (a disintegrin and metalloproteinase with thrombospondin motifs) family. Genome Biol. 16, 113.
Kim, W.R., Flamm, S.L., Di Bisceglie, A.M., Bodenheimer, H.C., Public Policy Committee of the American Association for the Study of Liver, D, 2008. Serum activity of alanine aminotransferase (ALT) as an indicator of health and disease. Hepatology 47, 1363–1370.
Kumar, B.S., Chung, B.C., Kwon, O.S., Jung, B.H., 2012. Discovery of common urinary biomarkers for hepatotoxicity induced by carbon tetrachloride, acetaminophen and methotrexate by mass spectrometry-based metabolomics. J. Appl. Toxicol. 32, 505–520.
Lin, S., Yang, Z., Zhang, X., Bian, Z., Cai, Z., 2011. Hippocampal metabolomics reveals 2,3,7,8-tetrachlorodibenzo-p-dioxin toxicity associated with ageing in Sprague-Dawley rats. Talanta 85, 1007–1012.
Locke, S.J., Brauer, M., 1991. The response of the rat liver in situ to bromobenzene—in vivo proton magnetic resonance imaging and 31P magnetic resonance spectroscopy studies. Toxicol. Appl. Pharmacol. 110, 416–428.
Luo, L., Aubrecht, J., Li, D., Warner, R.L., Johnson, K.J., Kenny, J., Colangelo, J.L., 2018. Assessment of serum bile acid profiles as biomarkers of liver injury and liver disease in humans. PLoS One 13, e0193824.
Ma, Z., Wang, X., Yin, P., Wu, R., Zhou, L., Xu, G., Niu, J., 2019. Serum metabolome and targeted bile acid profiling reveals potential novel biomarkers for drug-induced liver injury. Medicine 98, e16717.
Marcellin, P., Levy, S., Erlinger, S., 1997. Therapy of hepatitis C: patients with normal aminotransferase levels. Hepatology 26, 133S–136S.
Mardinoglu, A., Agren, R., Kampf, C., Asplund, A., Uhlen, M., Nielsen, J., 2014. Genome-scale metabolic modelling of hepatocytes reveals serine deficiency in patients with non-alcoholic fatty liver disease. Nat. Commun. 5, 3083.
McGill, M.R., Jaeschke, H., 2014. Mechanistic biomarkers in acetaminophen-induced hepatotoxicity and acute liver failure: from preclinical models to patients. Expert Opin. Drug Metab. Toxicol. 10, 1005–1017.
McGill, M.R., Jaeschke, H., 2019. Biomarkers of drug-induced liver injury. Adv. Pharmacol. 85, 221–239.

McGill, M.R., Staggs, V.S., Sharpe, M.R., Lee, W.M., Jaeschke, H., Acute Liver Failure Study Group, 2014. Serum mitochondrial biomarkers and damage-associated molecular patterns are higher in acetaminophen overdose patients with poor outcome. Hepatology 60, 1336–1345.
Minami, K., Saito, T., Narahara, M., Tomita, H., Kato, H., Sugiyama, H., Kato, H., Nakajima, M., Yokoi, T., 2005. Relationship between hepatic gene expression profiles and hepatotoxicity in five typical hepatotoxicant-administered rats. Toxicol. Sci. 87, 296–305.
Nallagangula, K.S., Nagaraj, S.K., Venkataswamy, L., Chandrappa, M., 2018. Liver fibrosis: a compilation on the biomarkers status and their significance during disease progression. Future Sci. OA 4, FSO250.
Nelson, S.D., 1990. Molecular mechanisms of the hepatotoxicity caused by acetaminophen. Semin. Liver Dis. 10, 267–278.
Origassa, C.S., Camara, N.O., 2013. Cytoprotective role of heme oxygenase-1 and heme degradation derived end products in liver injury. World J. Hepatol. 5, 541–549.
Ozer, J., Ratner, M., Shaw, M., Bailey, W., Schomaker, S., 2008. The current state of serum biomarkers of hepatotoxicity. Toxicology 245, 194–205.
Pannala, V.R., Wall, M.L., Estes, S.K., Trenary, I., O'Brien, T.P., Printz, R.L., Vinnakota, K.C., Reifman, J., Shiota, M., Young, J.D., Wallqvist, A., 2018. Metabolic network-based predictions of toxicant-induced metabolite changes in the laboratory rat. Sci. Rep. 8, 11678.
Pannala, V.R., Vinnakota, K.C., Rawls, K.D., Estes, S.K., O'Brien, T.P., Printz, R.L., Papin, J.A., Reifman, J., Shiota, M., Young, J.D., Wallqvist, A., 2019. Mechanistic identification of biofluid metabolite changes as markers of acetaminophen-induced liver toxicity in rats. Toxicol. Appl. Pharmacol. 372, 19–32.
Pannala, V.R., Vinnakota, K.C., Estes, S.K., Trenary, I., O'Brien, T.P., Printz, R.L., Papin, J.A., Reifman, J., Oyama, T., Shiota, M., Young, J.D., Wallqvist, A., 2020. Genome-scale model-based identification of metabolite indicators for early detection of kidney toxicity. Toxicol. Sci. 173, 293–312.
Pimentel, H., Bray, N.L., Puente, S., Melsted, P., Pachter, L., 2017. Differential analysis of RNA-seq incorporating quantification uncertainty. Nat. Methods 14, 687–690.
Pratt, D.S., Kaplan, M.M., 2000. Evaluation of abnormal liver-enzyme results in asymptomatic patients. N. Engl. J. Med. 342, 1266–1271.
Ramachandran, A., Jaeschke, H., 2018. Acetaminophen toxicity: novel insights into mechanisms and future perspectives. Gene Expr. 18, 19–30.
Ramachandran, R., Kakar, S., 2009. Histological patterns in drug-induced liver disease. J. Clin. Pathol. 62, 481–492.
Rawls, K.D., Blais, E.M., Dougherty, B.V., Vinnakota, K.C., Pannala, V.R., Wallqvist, A., Kolling, G.L., Papin, J.A., 2019. Genome-scale characterization of toxicity-induced metabolic alterations in primary hepatocytes. Toxicol. Sci. 172, 279–291.
Roshan, B., Guzman, G., 2014. Histological and clinical characteristics of patients with chronic hepatitis C and persistently normal alanine aminotransferase levels. Hepat. Res. Treat. 2014, 760943.
Sahini, N., Selvaraj, S., Borlak, J., 2014. Whole genome transcript profiling of drug induced steatosis in rats reveals a gene signature predictive of outcome. PLoS One 9, e114085.
Senior, J.R., 2012. Alanine aminotransferase: a clinical and regulatory tool for detecting liver injury-past, present, and future. Clin. Pharmacol. Ther. 92, 332–339.
Shi, Q., Hong, H., Senior, J., Tong, W., 2010. Biomarkers for drug-induced liver injury. Expert Rev. Gastroenterol. Hepatol. 4, 225–234.
Starkey Lewis, P.J., Dear, J., Platt, V., Simpson, K.J., Craig, D.G., Antoine, D.J., French, N.S., Dhaun, N., Webb, D.J., Costello, E.M., Neoptolemos, J.P., Moggs, J., Goldring, C.E., Park, B.K., 2011. Circulating microRNAs as potential markers of human drug-induced liver injury. Hepatology 54, 1767–1776.
Sturgill, M.G., Lambert, G.H., 1997. Xenobiotic-induced hepatotoxicity: mechanisms of liver injury and methods of monitoring hepatic function. Clin. Chem. 43, 1512–1526.
Thor, H., Orrenius, S., 1980. The mechanism of bromobenzene-induced cytotoxicity studied with isolated hepatocytes. Arch. Toxicol. 44, 31–43.
Thulin, P., Nordahl, G., Gry, M., Yimer, G., Aklillu, E., Makonnen, E., Aderaye, G., Lindquist, L., Mattsson, C.M., Ekblom, B., Antoine, D.J., Park, B.K., Linder, S., Harrill, A.H., Watkins, P.B., Glinghammar, B., Schuppe-Koistinen, I., 2014. Keratin-18 and microRNA-122 complement alanine aminotransferase as novel safety biomarkers for drug-induced liver injury in two human cohorts. Liver Int. 34, 367–378.
Vilar-Gomez, E., Chalasani, N., 2018. Non-invasive assessment of non-alcoholic fatty liver disease: clinical prediction rules and blood-based biomarkers. J. Hepatol. 68, 305–315.
Vinnakota, K.C., Pannala, V.R., Wall, M.L., Rahim, M., Estes, S.K., Trenary, I., O'Brien, T.P., Printz, R.L., Reifman, J., Shiota, M., Young, J.D., Wallqvist, A., 2019. Network modeling of liver metabolism to predict plasma metabolite changes during short-term fasting in the laboratory rat. Front. Physiol. 10, 161.
Wang, K., Zhang, S., Marzolf, B., Troisch, P., Brightman, A., Hu, Z., Hood, L.E., Galas, D.J., 2009. Circulating microRNAs, potential biomarkers for drug-induced liver injury. Proc Natl Acad Sci U S A 106, 4402–4407.
Waters, N.J., Waterfield, C.J., Farrant, R.D., Holmes, E., Nicholson, J.K., 2006. Integrated metabonomic analysis of bromobenzene-induced hepatotoxicity: novel induction of 5-oxoprolinosis. J. Proteome Res. 5, 1448–1459.
Watkins, P.B., 1992. Drug metabolism by cytochromes P450 in the liver and small bowel. Gastroenterol. Clin. North Am. 21, 511–526.
Young, J.D., 2014. INCA: a computational platform for isotopically non-stationary metabolic flux analysis. Bioinformatics 30, 1333–1335.
Yu, C., Woo, H.J., Yu, X., Oyama, T., Wallqvist, A., Reifman, J., 2017. A strategy for evaluating pathway analysis methods. BMC Bioinformatics 18, 453.